

# NIST-F1: recent improvements and accuracy evaluations\*

T P Heavner, S R Jefferts, E A Donley, J H Shirley and T E Parker

National Institute of Standards and Technology, Time and Frequency Division 847,  
325 Broadway, Boulder, CO 80305, USA

Received 18 March 2005

Published 13 September 2005

Online at [stacks.iop.org/Met/42/411](http://stacks.iop.org/Met/42/411)

## Abstract

In the last several years we have made many improvements to NIST-F1 (a laser-cooled Cs fountain primary frequency standard at the National Institute of Standards and Technology (NIST) in Boulder, Colorado) resulting in a reduction by over a factor of 2 in the uncertainty of the realization of the SI second. The two most recent accuracy evaluations of NIST-F1 had combined standard fractional uncertainties of  $0.61 \times 10^{-15}$  (June 2004) and  $0.53 \times 10^{-15}$  (January 2005), which were submitted to the Bureau International des Poids et Mesures with total fractional uncertainties (including time-transfer contributions) of, respectively,  $0.88 \times 10^{-15}$  and  $0.97 \times 10^{-15}$ . Here we discuss the improvements and evaluation methods and present an updated uncertainty budget.

## 1. Introduction

NIST-F1 is a laser-cooled Cs fountain primary frequency standard at the National Institute of Standards and Technology (NIST) in Boulder, Colorado [1]. In the last several years we have made many improvements to the NIST-F1 physics package and evaluation procedure resulting in a significantly improved accuracy budget compared with that presented in [1]. While the improvements individually appear minor, the net result has been significant. Since November 1999 NIST-F1 has undergone 14 formal frequency evaluations that have been submitted to the Bureau International des Poids et Mesures (BIPM) with combined standard fractional uncertainties of  $\approx 1 \times 10^{-15}$ . Recently we reported (January 2005) a combined standard fractional uncertainty of  $0.53 \times 10^{-15}$ , smaller by more than a factor of 2 than that reported in [1]. The previous evaluation of NIST-F1 (June 2004) had a combined standard fractional uncertainty of  $0.61 \times 10^{-15}$  and due to the long reporting interval (60 days) and resulting small time-transfer uncertainty, this evaluation was submitted to the BIPM with a total fractional uncertainty of  $0.88 \times 10^{-15}$ , the lowest ever reported by a primary frequency standard. The uncertainties in the Cs spin-exchange shift and the second-order Zeeman shift corrections have been reduced, and the blackbody shift is now the dominant item in the final systematic uncertainty budget. Here we report on the improvements and present in table 1 an updated uncertainty budget. While many of the

improvements and reconsidered frequency biases discussed in this paper have not had a significant impact on the NIST-F1 final uncertainty budget, they are included here since the BIPM requests that standards laboratories provide details concerning the operation of primary frequency standards that contribute to International Atomic Time (TAI).

The improved accuracy reported by NIST-F1 is largely due to three factors: the entire system is much more reliable; the Cs optical molasses has been improved; and the uncertainty in the second-order Zeeman correction has been re-evaluated. The improved system reliability has allowed for long, nearly uninterrupted operation resulting in the reduction of statistical uncertainties as well as the reduction of the uncertainties of systematic biases that are evaluated using Type A methods. Also, the ability to operate NIST-F1 for long periods is important for reducing the noise in the time-transfer process used to submit measurements to the BIPM and to compare directly with other primary standards. The Cs optical molasses in NIST-F1 has also been improved; it is presently about four times larger in volume and the atom temperatures are lower. Thus, NIST-F1 is able to operate at improved stabilities, since the fraction of detected atoms per launched ball of atoms is larger. This results in a smaller spin-exchange shift, since the density of the optical molasses is lower. Using the techniques described in [1] to evaluate the spin-exchange shift (which yields an uncertainty of approximately 20% of the bias) results in a reduction in the uncertainty. It is important to note [2] that the method by which the uncertainty in the spin-exchange

\* Work of the US government. Not subject to copyright.

**Table 1.** A new uncertainty budget for known frequency biases in NIST-F1 (units are fractional frequency  $\times 10^{-15}$ ). The magnitudes of the corrected biases are typical and are based on those obtained from the January 2005 evaluation of NIST-F1. The new Type B uncertainties for the biases are based on the discussions presented in this paper and will appear in future evaluations of NIST-F1 submitted into TAI. The frequency bias listed for the spin-exchange shift is for the lowest atomic density, at which NIST-F1 operates  $\sim 70\%$  to  $80\%$  of the time, depending on the schedule of a particular accuracy evaluation. The total uncertainty shown here does not include the spin-exchange uncertainty since it is added into the combined standard statistical fractional uncertainty as a Type A. Although the microwave leakage uncertainty was also evaluated using Type A methods, it is included in the total uncertainty because the measurements were made outside the accuracy evaluation timeframe.

Physical effect	Magnitude	Uncertainty	Evaluation technique (Type A or B)	Correction applied (Y/N)
Gravitational redshift	+180.54	0.03	B	Y
Second-order Zeeman	+36.53	0.02	B	Y
Blackbody	-21.21	0.26	B	Y
Spin exchange at low density	-0.42	0.10	A	Y
Microwave leakage	0	0.20	A	N
ac Zeeman (heaters)	0.05	0.05	B	N
Cavity pulling	0.02	0.02	B	N
Rabi pulling	$10^{-4}$	$10^{-4}$	B	N
Ramsey pulling	$10^{-4}$	$10^{-4}$	B	N
Majorana transitions	0.02	0.02	B	N
Fluorescence light shift	$10^{-5}$	$10^{-5}$	B	N
Cavity phase (distributed)	0.02	0.02	B	N
Second-order Doppler	0.02	0.02	B	N
The dc Stark effect	0.02	0.02	B	N
Background gas collisions	$10^{-3}$	$10^{-3}$	B	N
Bloch-Siegert	$10^{-4}$	$10^{-4}$	B	N
RF spectral purity	$3 \times 10^{-3}$	$3 \times 10^{-3}$	B	N
Integrator offset	0	0.01	A	N
Total uncertainty (not including spin exchange)		0.35		

shift in NIST-F1 is reported has varied as our understanding of the evaluation of the bias has matured. The uncertainty has been reported as either Type A or Type B (this has no effect on the combined uncertainty). Despite how it has been reported, the total magnitude of the uncertainty has decreased with improvements to NIST-F1. The third major factor that has improved the accuracy is the reduction in the uncertainty in the second-order Zeeman correction. As described in [1], the fractional uncertainty of  $0.3 \times 10^{-15}$  corresponds to an uncertainty in the location of the central fringe on the  $|3, 1\rangle \rightarrow |4, 1\rangle$  manifold of  $\pm 1$  fringe. In fact, the measurements are much better than this, and this very conservative uncertainty has been reduced.

Figure 1 is a long-term Allan deviation plot obtained from NIST-F1 that highlights the impact of the recent improvements. This plot compares NIST-F1 against AT1E, a post-processed NIST timescale generated by five cavity-tuned hydrogen masers and four high-performance commercial Cs beam standards. The Allan deviation shows white FM noise properties out to 24 days, where the stability is measured to be  $\sigma_y \sim 4 \times 10^{-16}$ . This result complements and is consistent with other independent measurements [3], which showed the noise level of AT1E to be substantially lower than that in figure 1, except at large  $\tau$ , where the stability of AT1E is  $\sigma_y \sim 3 \times 10^{-16}$  for averaging times of 10 days. NIST-F1 operates most often at a low atom density, and this sets the noise level shown in this plot. For reference, the present stability at low atom density is comparable to the previous stability of NIST-F1 at high atom density shown in figure 10 of [1]. There has also been some improvement due to changes in the microwave synthesis chain discussed here in section 2.5.

The measurement of the performance of NIST-F1 against the timescale AT1E shows that the Type A (statistical)

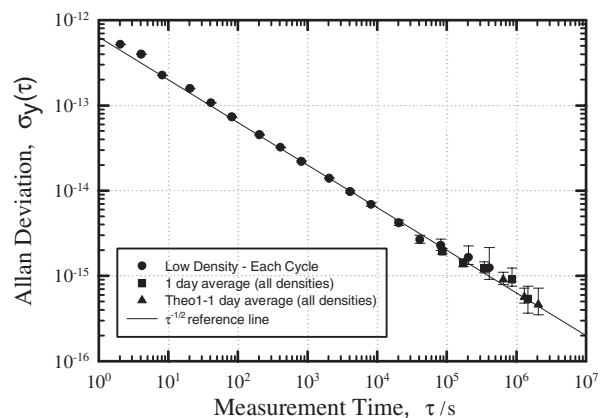


**Figure 1.** An Allan deviation plot comparing NIST-F1 against AT1E demonstrates white FM noise properties out to 24 days, where the stability is estimated as  $\sigma_y \sim 4 \times 10^{-16}$ . The data at short sampling times were obtained by calculating the Allan deviation of frequency measurements from 14 days of continuous fountain operation at low atomic density. The Allan deviation at longer sampling times was calculated using the 24 h average frequency of all individual runs. Measurements taken at high atomic densities, where the stability is better, have been included by removing the frequency offset due to the spin-exchange shift. Several points at long sampling times were calculated by use of Theo-1, a statistic designed to increase the confidence at the largest  $\tau$  values.

uncertainties obtained during evaluations are valid and confirms our methods used to measure the Cs spin-exchange shift. Specifically, the technique of varying the atomic density over the period of days to evaluate the bias is statistically rigorous since the combined fountain and ensemble noise is still white in character. The high reliability exhibited by NIST-F1, resulting in long ( $\sim 40$  days), nearly uninterrupted

runs, facilitated the analysis of long-term behaviour shown in figure 1. Note that the last few points at the largest  $\tau$  values were calculated using Theo-1, a statistic designed to increase the confidence at large  $\tau$  values [4]. A more detailed discussion on how the timescale AT1E is used during accuracy evaluations to measure and correct for the spin-exchange shift appears in a separate publication [2]. Specifically, that work describes the statistical methods used to extrapolate frequency measurements to zero density and the determination of the associated uncertainties.

The nine sections of this paper describe the current state of NIST-F1 and the evaluation methodology. Section 2 describes the improvements that have been made to the NIST-F1 physics package, laser and optics system and control system. The role of the NIST timescale, AT1E, in the evaluations of NIST-F1 is described in section 3. The systematic shifts that are corrected for during the evaluations of NIST-F1 are discussed in section 4. Section 5 is an updated discussion of systematic shifts that were determined in [1] to be negligible and have since been re-evaluated as the fractional uncertainties of NIST-F1 approach  $1 \times 10^{-16}$ . This re-evaluation of small biases is also important for NIST-F2, the second-generation Cs fountain now under development at NIST. A typical evaluation procedure for NIST-F1 is outlined in section 6. Section 7 describes how the noise in the time-transfer process impacts our evaluation techniques. Finally, in section 8 we compare the performance of NIST-F1 against other Cs fountain primary standards that have contributed to TAI, and we summarize in section 9.

## 2. Improvements made to NIST-F1

### 2.1. Overview

In the last two years, the NIST-F1 physics package has undergone several major maintenance and upgrade procedures (new Cs ovens, graphite getters, etc) that required breaking vacuum and the disassembly of major components. During the repairs, improvements were made to the apparatus. The laser system described in [1] was replaced in 2002 with a commercial system, and the optics layout was improved. A new control system was implemented that monitors the health of many sub-systems and notifies the user when faults are detected. This has made NIST-F1 a more reliable and robust apparatus capable of long uninterrupted run times. Most recently, a new generation microwave synthesizer has been incorporated into the NIST-F1 system. We have found no evidence that the upgrades have resulted in any bias in the evaluated accuracy of NIST-F1. Even though work has begun on the second-generation NIST fountain, NIST-F2, we plan to continue improving NIST-F1. Table 2 shows the operating parameters presently used in NIST-F1. A comparison with the parameters from [1] reveals the use of larger beams with higher intensity in the optical molasses, a lower atom temperature and a lower magnitude for the C-field.

### 2.2. Laser and optics

Since the publication of [1], the NIST-F1 laser system and the optical layout have changed considerably. Both the main laser, used for the optical molasses and detection, and the

**Table 2.** General operating parameters for NIST-F1 at low atom density. Values are approximate.

Parameter	Value
Molasses load time	80 ms to 500 ms
Total atom number gathered and tossed	$\sim 10^6$
Number of atoms in $m_F = 0$	$\sim 10^5$
Number detected	$\sim 10^4$
Atom temperature	$\sim 0.5 \mu\text{K}$
Standard launch velocity	$4.26 \text{ m s}^{-1}$
Standard Ramsey time	0.56 s
Optical power (horizontal beams)	$\sim 50 \text{ mW}$
Beam diameter (horizontal beams)	$\sim 2.5 \text{ cm}$
Optical power (vertical beams)	$\sim 10 \text{ mW}$
Beam diameter (vertical beams)	$\sim 1 \text{ cm}$
One measurement cycle period	2.2 s
C-field	$0.085 \mu\text{T}$
Detection beam intensity/ $I_{\text{Saturation}}$	$\sim 1$

repump laser have been replaced. Originally, the NIST-F1 laser system consisted of an extended cavity diode laser (ECDL) pumped master oscillator power amplifier (MOPA) operating at 852 nm. The light was then divided and sent to acousto-optical modulator (AOM) frequency shifters to generate the beams needed for the optical molasses and detection. All light was delivered to the fountain physics package by use of free-space beams, i.e. without the use of fibre optic cables. The repump laser was based on a distributed Bragg reflector (DBR) diode, and the light was also delivered via a free beam to the physics package. All the laser sources and optical processing were performed on the same table upon which the fountain physics package resides. Due to the close proximity of high power resonant light sources to the physics package, several mechanical shutters and stray light baffles were used to avoid light shifts.

Because of concerns over the long-term availability of 852 nm diodes from industry and the peculiarities associated with our ECDL systems, we decided to replace the main laser with a commercial laser package. This system consists of a diode-pumped, frequency-doubled Nd:YVO<sub>4</sub> laser and provides  $\approx 10 \text{ W}$  of 532 nm light that pumps a Ti:sapphire ring laser to generate  $\approx 1 \text{ W}$  of narrow band light at 852 nm. The original repump laser was replaced due to diode failure. While the new repump system still uses 852 nm diodes, it supplies more power and is housed in a superior mechanical package that has improved the reliability and reduced the possibility of light shifts, since all optical processing occurs within this enclosure. This system uses an 852 nm DBR diode to injection lock a higher-power 852 nm diode to provide  $\sim 50 \text{ mW}$  of light that exits the laser package through a polarization-maintaining (PM) fibre optic cable.

Both laser sources are now located on an optical table across the laboratory from the fountain physics package, and the light is delivered using PM fibre optic cables. Before the beams are injected into the fibre optic cables, they pass through a new mechanical shutter assembly that blocks the light during Ramsey interrogation. Now, as opposed to the previous layout described above, there is never any resonant light on the table holding the fountain physics package during Ramsey interrogation. Also, the use of fibre optic cables has resulted in a more stable optical system since the fibre output coupler is mechanically fixed. Thus, changes in the beam at the laser

output only require that the fibre input injection be re-optimized rather than the entire optical table.

The design of the mechanical light shutter has been greatly improved. The previous generation of light shutters was based on mechanical irises and exhibited poor reliability. Presently, each assembly consists of a pair of closely spaced shutter blades separated by a small aperture. A shutter is made from a 1 cm × 4 cm piece of thin stainless steel shim stock with one end mounted to the shaft of a stepping motor. The position of the shutter blades is controlled using the stepping motor, which receives open and close commands from the fountain control system. On the output side of each fibre, there is a photodiode monitor connected to the control system. This system looks for shutter failures in each fountain measurement cycle by measuring the signal level on the photodiode monitor when the shutters are commanded to be closed. A shutter fault, which would result in resonant light appearing on the optical table that holds the physics package during Ramsey interrogation and possibly a resonant light shift, is logged by the main control software. That measurement cycle can be rejected in the final analysis of the data. More importantly, a faulty shutter is detected immediately, resulting in a minimum of dead time. This system is redundant since the monitor photodiode is mounted on yet another shutter blade that drops into the beam when the main shutter is closed. So, even if the main shutter fails, the monitor shutter will block the light.

While this new shutter system is a significant improvement over the previous generation, it is not without flaws which need to be addressed. The shutter monitor system is optimized to detect glitches in the opening or closing of the shutters. However, if the shutter holding the monitor photodiode becomes permanently stuck in the open position, or if both shutters become stuck in the open position, the monitor system cannot detect these errors. However, such gross shutter failures are evident because of the large fluorescent light shift. Nevertheless, we plan to further modify the shutter system to address these issues.

Both new laser systems have displayed a high level of reliability with lock times measured in weeks. This reliability has improved our measurement statistics since our ‘live time’, the fraction of time in which useful data are collected divided by the intended run time, is presently ~97%. This is now limited by planned shutdowns to tune up optics, change the oven temperature, maintain software, or deal with rare failure modes that have not been addressed in our recent upgrades. In early evaluations typically 90% of the dead time was caused by laser problems, whereas in our evaluation of June 2004 no dead time was due to the lasers.

### 2.3. Optical molasses

Compared with the previous system, more than twice the useful laser light power is available from the new laser system. This has allowed for larger horizontal beams in the (0, 0, 1) molasses geometry, while still providing enough intensity for a good optical molasses. (Although the vertical beams have more power, they are the same size since they are defined by the apertures in the microwave cavities.) New magnetic field compensation coils around the molasses region have improved the uniformity of the magnetic field in the centre of the source

region. The net result is a larger optical molasses in the vertical dimension with improved uniformity and stability. This allows for fountain operation with a 50% smaller spin-exchange shift, (lower density) without loss of stability, which depends on total atom number detected. Finally, we obtain very low atom velocity distributions which correspond to temperatures of ~0.5 μK, attributed to the above improvements as well as to experience gained over the years in optimizing other parameters such as the post-cool applied immediately after launch.

### 2.4. Detection region

Several improvements have been made to the atom detection region in NIST-F1. As described in [1], the two-zone detection region uses a sequence of spatially separated sheets of resonant laser light to measure the populations of the  $F = 4$  and  $F = 3$  states in a ball of atoms as they exit the microwave interrogation region. The original vacuum windows that allow the probe beams into the detection zone (which were uncoated) were replaced with windows coated for 852 nm. This has significantly reduced the noise due to scattered light. Furthermore, the detection laser light level is now servo-controlled, and this has reduced high-frequency laser-intensity noise as well as long-term drift in the intensity. The shot-to-shot noise in the detection system is now lower and the quantum projection noise limit is reached at  $\approx 3 \times 10^3$  detected atoms. Also, reduction in the long-term drift in the detection light intensity has improved the calibration of atom number and thus has improved the evaluation of the Cs spin-exchange shift.

### 2.5. Microwave synthesis chain

The microwave synthesis chain has undergone several changes since the publication of [1]. The highlights discussed here are (1) the addition of a high-quality quartz crystal oscillator that serves to reduce short-term noise (above ~0.02 Hz) from the reference maser; (2) the employment of additional synthesizers operating in parallel with the main synthesizer and that serve as sensitive phase noise monitors; and (3) the recent conversion to a new clock transition synthesizer (9.193 GHz) based on simpler, yet superior dielectric resonant oscillators (DROs).

In the past, the short-term stability of NIST-F1 was degraded by noise from the maser. The addition of a high-quality quartz crystal obtained from Oscilloquartz<sup>1</sup> in a phase-locked loop ( $\tau \approx 10$  s) between the reference maser and the NIST-F1 microwave synthesizer reduced this noise (above ~0.02 Hz) from the maser. This circuit topology exhibits the superior short-term performance of the quartz crystal while maintaining the long-term stability of the maser.

We have observed in the past that synthesizer errors that are sensed by the Cs atoms may not be easily detected by the lock monitoring electronics. Figure 2 shows a second, parallel synthesis chain that serves as an error monitor. While this dual system cannot determine which half of the synthesis chain is at fault, it is very sensitive at detecting a fault in either system and is a good indicator of overall synthesizer

<sup>1</sup> The trade name Oscilloquartz is identified for completeness of technical description and does not constitute or imply endorsement.

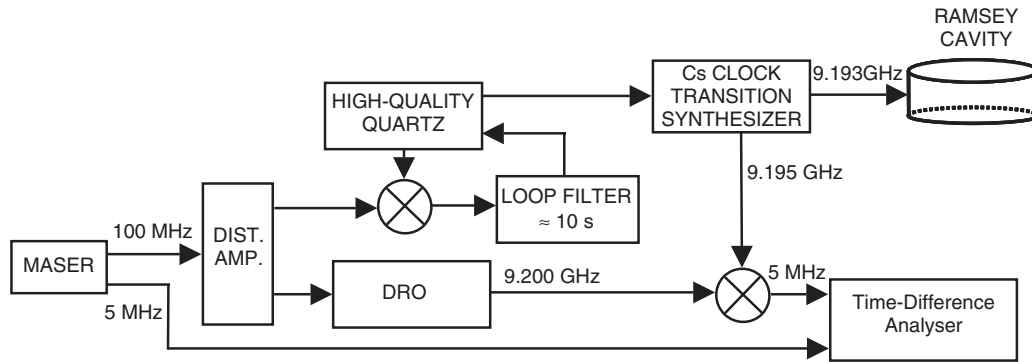


**Figure 2.** A schematic diagram showing the key components of the synthesis chain used to generate microwaves at 9.193 GHz and the associated monitoring system. A 100 MHz signal from a maser in the NIST clock ensemble is used in two separate microwave synthesis chains. In the upper path, a high-quality quartz oscillator is phase-locked to the 100 MHz reference ( $\sim 10$  s time-constant) to remove fast noise from the maser. This is fed into the NIST-F1 synthesizer, which generates 9.193 GHz to interrogate the Cs clock transition. The lower chain serves as a sensitive error detection system. The 100 MHz signal is fed into a DRO that produces 9.200 GHz. The 5 MHz beat note between this and a 9.195 GHz signal derived from the NIST-F1 synthesizer is compared with a 5 MHz signal from the maser using a commercial time-difference analyser.

performance. The 100 MHz reference from the maser is fed into both chains. The first chain contains the Oscilloquartz crystal and the synthesizer module used to generate 9.193 GHz used for Ramsey interrogation. The second chain uses a DRO to produce 9.200 GHz from the 100 MHz reference. A mixer is used to beat the 9.200 GHz against a 9.195 GHz signal derived from the NIST-F1 synthesizer and the resulting 5 MHz signal is fed into a commercial instrument that records the phase difference once per second between the 5 MHz from the synthesizer and the 5 MHz directly from the maser. Any errors in the synthesis chain will appear in the phase difference measurements and that will indicate that maintenance of the synthesizer is required. Figure 3 shows that the Allan deviation between the two 5 MHz signals reaches a stability of  $\sigma_y \sim 1.1 \times 10^{-13}$  at one fountain cycle ( $\sim 2$  s) and falls off at  $\sim \tau^{-1}$  down to  $\sigma_y \sim 1.3 \times 10^{-17}$  at  $\tau \sim 4 \times 10^5$  s. This noise floor is below the quantum projection noise stability level at which NIST-F1 is operated. This system has been employed in NIST-F1 from approximately 2003 to 2004.

Until recently, the synthesizer used to generate microwaves at 9.193 GHz was based on a topology that had been previously used by NIST on both NIST-F1 and NIST-7 [5]. This main synthesizer was recently replaced with a system shown in figure 4, which uses a much simpler architecture. The system is based on a DRO operating at 9.2 GHz and which is mixed with 7.368 230 MHz from a direct digital synthesis (DDS) module in a single-sideband (SSB) mixer to produce microwaves at the Cs clock transition (see section 5.9).

## 2.6. Vacuum system

A new vacuum manifold has been added to the fountain physics package and contains both a second ion pump and a second titanium-sublimation pump. While the pumping speed out of the Cs source region is not significantly different with this new manifold, due to the conductance-limiting geometry, there is an increase in pump capacity. Also, a sensitive ion gauge with a base pressure of  $5 \times 10^{-12}$  Torr ( $6.6 \times 10^{-10}$  Pa) was added to the physics package below the molasses region. This is used in conjunction with ion pump current readings to determine the pressure within the physics package. The

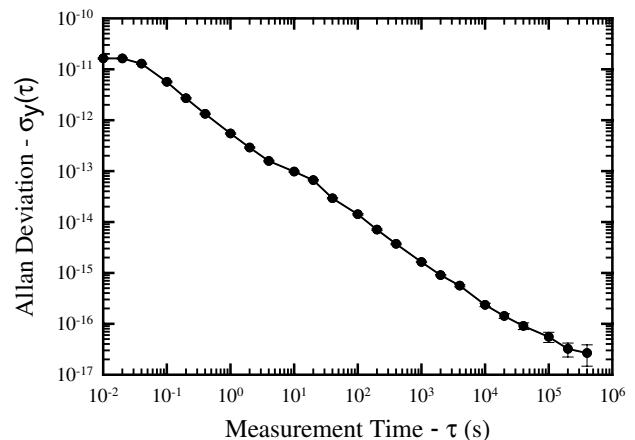


**Figure 3.** An Allan deviation plot of the two 5 MHz signals fed into the time-difference analyser in the microwave monitoring system illustrating that the microwave synthesizer is a negligible noise source in NIST-F1. The y-axis has been scaled to show the fractional frequency stability referenced to the 9 GHz sources. The stability at  $\sim 4 \times 10^5$  s is below  $3 \times 10^{-17}$ .

addition of the ion gauge has been useful since pressure readings from ion pumps can be unreliable in vacuum systems containing caesium. Although this ion gauge is below the optical molasses region, it provides a good measure of the pressure within the Ramsey interrogation region above the source region due to the symmetry in the physics package, i.e. the conductance between the ion gauge and the pumps is the same as between the Ramsey interrogation region and the pumps, and the Cs gas load is the same for both locations. This new vacuum instrumentation gives us added confidence in determining any possible frequency bias due to background gases (see section 5.11).

## 2.7. C-field uniformity and mapping

New magnetic field shims were added in the region of the microwave cavities where magnetic field inhomogeneities are present due to the significant mass of the copper structure. This is a minor issue since the atoms spend very little time in this

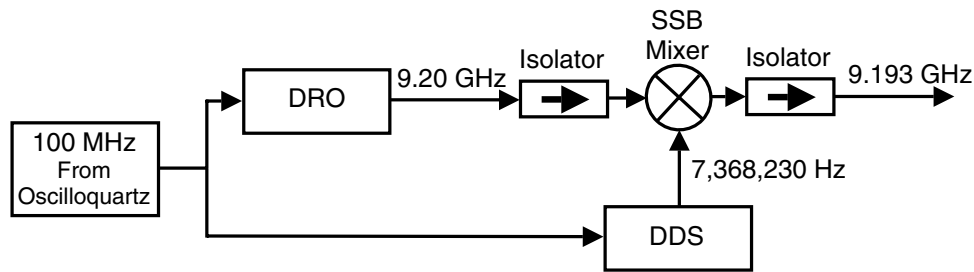


**Figure 4.** A schematic layout of the most recent microwave synthesizer developed for NIST-F1. A 100 MHz reference signal is fed to a DRO module that multiplies by 92 up to 9.20 GHz. This is mixed with an RF signal at 7.368 23 MHz from a DDS unit, also referenced to the 100 MHz, in an SSB mixer to produce microwaves at the Cs clock transition.

portion of the magnetic field. Nevertheless, the new shim coils allow finer adjustments to be made to the C-field.

### 2.8. Temperature control

The temperature of the Ramsey interrogation region of NIST-F1 is controlled to maintain the cavity resonance to much less than one linewidth from the Cs clock transition and also to correct for the blackbody shift. Several improvements have been made to the temperature control system. Improved temperature-sensing instrumentation was added along the microwave cavity and copper flight tube, including a Pt resistance temperature detector (RTD) that has an accuracy of  $\pm 0.1$  K. Also, heater winding configurations were improved to reduce temperature gradients.

Until the end of 2003, the heater windings were operated in a pulsed excitation mode to avoid the possibility of a second-order Zeeman shift. (Since the heaters operated at 25 kHz, the effect is an ac second-order Zeeman shift.) That is, the heaters were on during optical molasses and off during Ramsey interrogation. Recently, a re-analysis of this configuration gave insight into a frequency shift not yet considered [6]. In the pulsed heater mode, the cavity temperature is well controlled in the long term because the thermal time constant of the copper structure is much greater than the period of the heater cycle. However, this periodic, small impulse of heat into the cavity structure can have a significant impact upon the phase of the microwave field within the cavity. Since the phase is perturbed at the beginning of every fountain cycle and is recovering during Ramsey interrogation, there is a dynamic end-to-end cavity phase shift. Our analysis presented in [6] showed this did not cause a problem at the reported  $\sim 10^{-15}$  accuracy level of NIST-F1. Nevertheless, our new approach has been to operate the ac heaters continuously and evaluate the resulting ac second-order Zeeman shift. A small dc current was added to the ac heater current while the frequency at the  $|3, 1\rangle \rightarrow |4, 1\rangle$  field-dependent transition was monitored. This showed the magnetic field generated by the heater windings to be  $\sim 7 \times 10^{-7} \text{ T A}^{-1}$ . This factor is small since the windings are in the form of dual conductor cables with opposite current directions to make zero magnetic field to first order. Also, the magnetic field as seen by the atoms due to the ac heater current operating at 25 kHz is diminished by  $\sim 10^3$  due to eddy-current shielding by the copper vacuum walls. The resulting fractional second-order ac Zeeman shift after considering these effects is  $4.3 \times 10^{-17}$ .

### 2.9. Control system

NIST-F1 uses a state machine architecture controlled by a high-speed digital pattern generator and, until the end of 2003, C++ based software was used to acquire the atom signals and operate the line-centre servo. The software, described in [1], was originally developed for NIST-7 and modified for NIST-F1. While we have much experience with this software and are confident of its performance, it was rather difficult to modify to make significant changes in the operation of NIST-F1. Therefore, we developed and are presently using new control routines written with a commercial graphical development software package that is much more flexible. New ideas and schemes can be implemented without long downtimes to reprogram the software. Also, the new control software architecture has superior error monitoring in the form of digital inputs that represent the health and status of many subsystems. The software sends emails or makes phone calls to the operators when gross errors or faults are detected, such as the loss of atom signal. This allows us to fix problems quickly, thus increasing the 'live time'. In addition to the line-centre servo, the new software also operates the atom-number servo, which is used in the evaluation of the Cs collisional shift. This servo measures the total number of atoms returning to the detection region and adjusts the microwave power entering the state-selection cavity to keep the atom number fixed to a set point.

## 3. NIST timescale

Recent measurements of the stability of NIST-F1 against AT1E showing white FM noise characteristics out to 24 days were presented in section 1. Here we discuss the role of AT1E in the operation of NIST-F1, while details are found in [2] including the statistical methods used to evaluate the spin-exchange bias and uncertainty. The NIST clock ensemble consists of five cavity-tuned hydrogen masers and four high-performance, commercial caesium standards and is used to generate AT1E, a post-processed timescale. In addition to the properties shown in figure 1, complementary measurements show AT1E to have a long-term frequency drift rate of less than  $\pm 3 \times 10^{-15}$  per year [3]. Because AT1E is exceptionally stable and its noise properties have been characterized, we are able to operate NIST-F1 using methods inaccessible to other fountain groups. Specifically, more dead time in the operation of NIST-F1 can be tolerated than if a single maser was used [7]. As a result, many different sequences of data separated by

dead time can be combined and treated as a single data set. Though the reliability of NIST-F1 has improved substantially and there is less unintentional dead time, the stability of AT1E can still be used to our advantage by stretching an evaluation by deliberately adding dead time to both ends of the evaluation in order to reduce the time-transfer uncertainty (see section 7).

The stability of AT1E is also important in the evaluation of the Cs spin-exchange shift [2]. NIST-F1 is operated at a fixed density (low, medium or high) for many days at a time. Without the long-term stability of AT1E, we would have to alternate much more rapidly between different densities. In some cases this would limit the range of densities we can achieve since it requires changes in the oven temperature and laser power to reach the highest densities. The performance of the fountain stabilizes only after periods of several hours, thus making rapid switching between densities impractical.

## 4. Corrected systematic frequency biases

### 4.1. Spin-exchange shift

Through the history of NIST-F1 several different techniques have been used in the evaluation of the Cs spin-exchange shift. This has been in response to the evolving knowledge concerning the nature of the shift. Originally in NIST-F1, the density of the atom cloud was measured and a correction was made to the clock frequency using published spin-exchange coefficients. However, results [8] showed that the frequency shift depends strongly on energy, and thus is a function of the type of Cs source used (MOT, molasses), and on details of the atomic velocity and spatial distributions. Thus, the shift needs to be measured for a particular fountain apparatus. But, given that these parameters remain constant, the shift is expected to be linear with atomic density. Though we no longer use published spin-exchange coefficients, we have found that the spin-exchange shifts of the evaluations based on published coefficients are within the experimentally observed spin-exchange uncertainties of later evaluations.

Presently, we use the density extrapolation method as described in [1] to measure the spin-exchange shift during each evaluation of the accuracy of NIST-F1. The frequency is measured at various atomic densities and a weighted, least-squares linear fit of the data yields an intercept and a slope that are used to determine the clock transition frequency at zero density. The density is set by controlling the detected atom signal. Measurements of the atomic spatial and velocity distributions in NIST-F1 show they are constant at  $\sim 1\%$  over the range of parameters used to change the atom number and confirm that the detected signal level is proportional to the atomic density. The detected atom signal level, or atom number, is controlled using two methods. For coarse changes (a factor of  $\sim 10$ ) in the atom number, small changes are made to the Cs oven temperature, molasses load time and laser power. Fine control ( $\sim 1\%$ ) is achieved using a servo that locks the detected atom signal to a set point by varying the microwave power entering the state-selection cavity. At all densities, the nominal set point on the microwave power is approximately the same to avoid any of the effects discussed in [9], whereby

microwave field inhomogeneities across the cavity aperture may result in a microwave power-dependent atom spatial distribution. The recent changes made to the molasses laser beam sizes and powers altered the dynamics of the spin-exchange shift observed in NIST-F1. However, the slopes from density extrapolations obtained during different evaluations but with the same basic optical molasses parameters have been in agreement within the uncertainties of the measurements.

We operate NIST-F1 with very low atomic densities such that the spin-exchange shift is very small and about the same size as the final total uncertainty. Although the stability is poor at low density, this regime is a good compromise between the density extrapolation method and the time-transfer noise. At high density ( $\sigma_y(\tau) \sim 2 \times 10^{-13} \tau^{-1/2}$ ), a small Type A uncertainty of  $\sim 5 \times 10^{-16}$  can be reached in a few days. To reach the same Type A uncertainty at low density ( $\sigma_y(\tau) \sim 6 \times 10^{-13} \tau^{-1/2}$ ) requires  $\sim 20$  days of operation. However, to reduce the uncertainty in the time-transfer process to  $\sim 1 \times 10^{-15}$ , we need to run the fountain for  $\sim 30$  days. Therefore, we operate most of the time ( $\sim 70\%$  to  $80\%$ ) at a low density where the fractional spin-exchange shift is  $\sim 0.5 \times 10^{-15}$ . An added advantage of operating in this regime is that we expect to achieve extended lifetimes from the Cs oven and the laser system, which runs well below its rated output power.

To rigorously reflect the evaluation method, we have changed the method in which we report the uncertainty in the spin-exchange shift [2]. The spin-exchange shift is a systematic shift like the second-order Zeeman and blackbody shifts, and is commonly reported as a Type B correction and uncertainty. However, Type A and Type B refer to the methods used to measure the physical quantity [10]. For example, the blackbody shift correction is made using measurements of the temperature environment as seen by the atoms in conjunction with a theory of the effect that uses Cs polarizability coefficients obtained from other experiments. The gravitational redshift correction is made in a similar fashion. Neither shift is actually directly measured during an evaluation. Since the density extrapolation technique is a statistical method, and the shift is measured during the evaluation, the spin-exchange shift correction falls into the Type A category. The uncertainty in the intercept obtained from the weighted, linear least-squares fit of the evaluation data is entirely a Type A uncertainty. It can be viewed as having a contribution from the uncertainty in the frequency measurements and a contribution from the uncertainty in the spin-exchange shift. In the past, our methods with which the spin-exchange shift was reported were not always consistent with this viewpoint. That is, the result of the extrapolation was artificially split into Type A and Type B contributions to incorrectly force the results into a standard format. Our evaluation reports now contain a single Type A uncertainty that includes the statistical uncertainty and a component due to the spin-exchange shift. There is no separate Type B uncertainty corresponding to the spin-exchange shift. It is important to note that the current combined Type A uncertainty (statistical and spin exchange) is consistent with our previous evaluations. It is only the fashion in which the total has been appropriated between the two types of uncertainties that has changed. Nevertheless, our evaluation reports contain a comment to

**Table 3.** A comparison of the July 2001 accuracy evaluation of NIST-F1 with the more recent June 2004 and January 2005 accuracy evaluations that highlights the improvements discussed in this paper (units are fractional frequency  $\times 10^{-15}$ ). Here  $u_A$  ( $u_{\text{Intercept}}$ ) is the uncertainty in the intercept (zero density) obtained from the extrapolation of atomic density versus frequency measured during the accuracy evaluations. As described in [2],  $u_A$  is the quadrature sum of  $u_{\text{Statistical}}$  and  $u_{\text{Spin-Exchange}}$ . The uncertainty  $u_{\text{Statistical}}$  is due to fountain noise and is the combined standard uncertainty of all the frequency measurements. The uncertainty  $u_{\text{Spin-Exchange}}$  is due to the systematic bias from the spin-exchange shift. Since the spin-exchange bias is measured during the accuracy evaluations using Type A methods, it is included in  $u_A$ . All other systematic biases are included in the uncertainty  $u_B$ . Several of these systematic biases are also evaluated using Type A methods, but are included in  $u_B$  since the measurements are performed outside the timeframe of the reported accuracy evaluations. The combined standard uncertainty,  $u_C$ , is the quadrature sum of  $u_A$  and  $u_B$ . Dead time (either intentional or unintentional) during the comparison of NIST-F1 against a reference maser in the NIST timescale contributes an uncertainty  $u_{\text{Link/Lab}}$ . The time-transfer used to submit the NIST-F1 frequency measurements to the BIPM has an uncertainty  $u_{\text{Link/TAI}}$  and the final uncertainty which appears in TAI,  $u_{\text{Total}}$ , is the quadrature sum of  $u_C$ ,  $u_{\text{Link/Lab}}$  and  $u_{\text{Link/TAI}}$ . Dead time is often added to both the beginning and end of an accuracy evaluation of NIST-F1 thus increasing  $u_{\text{Link/Lab}}$ . However, since  $u_{\text{Link/TAI}}$  continues to decrease as the length of the comparison interval increases, there is an overall reduction in  $u_{\text{Total}}$  [2].

	July 2001	June 2004	January 2005
$u_A = u_{\text{Intercept}} = \sqrt{u_{\text{Statistical}}^2 + u_{\text{Spin-Exchange}}^2}$	1.20	0.51	0.41
$u_{\text{Statistical}}$	0.86	0.28	0.25
$u_{\text{Spin-Exchange}}$	0.84	0.43	0.33
$u_B$	0.52	0.33	0.34
$u_C = \sqrt{u_A^2 + u_B^2}$	1.31	0.61	0.53
$u_{\text{Link/Lab}}$	0.24	0.40	0.30
$u_{\text{Link/TAI}}$	0.75	0.50	0.75
$u_{\text{Total}} = \sqrt{u_C^2 + u_{\text{Link/Lab}}^2 + u_{\text{Link/TAI}}^2}$	1.53	0.88	0.97

illustrate both the size of the spin-exchange shift and the uncertainty at the low density value at which the fountain operates  $\sim 70\%$  to  $80\%$  of the time, depending on the schedule of a particular accuracy evaluation. For the January 2005 evaluation of NIST-F1, the fractional spin-exchange shift at the lowest density was  $-0.42 \times 10^{-15}$  with an uncertainty of  $0.10 \times 10^{-15}$ .

To illustrate how improved statistics and a larger optical molasses have reduced the uncertainty of the spin-exchange shift, compare the results of the July 2001 with the June 2004 evaluation shown in table 3. The July 2001 evaluation, the results of which are described in [1], had an uncertainty in the intercept of  $1.2 \times 10^{-15}$ , of which the statistical component was  $0.86 \times 10^{-15}$  and the component due to the spin-exchange shift was  $0.84 \times 10^{-15}$ . For the June 2004 evaluation, the uncertainty in the intercept was  $0.51 \times 10^{-15}$  with a statistical component of  $0.28 \times 10^{-15}$  and a spin-exchange component of  $0.43 \times 10^{-15}$ .

#### 4.2. Second-order Zeeman shift

In [1] we described the methods for determining the second-order Zeeman shift correction in NIST-F1. Two complementary methods were described, and they are used to verify the results of one another. The first method involves generating a magnetic field map using the  $|3, 0\rangle \rightarrow |3, 1\rangle$  field-dependent transitions. The other method determines the central fringe on the  $|3, 1\rangle \rightarrow |4, 1\rangle$  manifold, and the field map is used to verify the measured frequency. Either method is valid and robust for determining the second-order Zeeman correction. In [1] we applied an uncertainty in the determination of the central fringe on the  $|3, 1\rangle \rightarrow |4, 1\rangle$  manifold to  $\pm 1$  fringe. This was a very conservative uncertainty since the two methods agree to within  $0.04 \pm 0.05$  fringes. Also, we have recently been operating NIST-F1 with a C-field  $\sim 20\%$  smaller in value than reported in [1] of  $\sim 0.1 \mu\text{T}$ . Given these facts, we now state an uncertainty

on the second-order Zeeman shift of  $< 2 \times 10^{-17}$ , which corresponds to  $\pm 0.1$  of a fringe. Long-term measurements on the  $|3, 1\rangle \rightarrow |4, 1\rangle$  transitions show a level of magnetic field noise corresponding to a fractional frequency shift of  $< 1 \times 10^{-17}$  on the  $|3, 0\rangle \rightarrow |4, 0\rangle$  transition. Nevertheless, as a precaution against undetected magnetic field perturbations, we are in the process of modifying the control software to monitor the field-dependent transition at regular intervals during an evaluation.

#### 4.3. Blackbody shift

While we have improved the temperature-sensing instrumentation and reduced temperature gradients along the copper microwave cavity and time of flight structure, the uncertainty in the blackbody shift in NIST-F1 still reflects a  $\pm 1$  K uncertainty in the radiation environment as seen by the atoms. A significant reduction in the uncertainty of the blackbody shift will require either major changes in the fountain physics package or revisiting the theory and the analysis that is presently used to calculate the shift. Recent work described in [11] calls into question the current theory and atomic polarizability coefficients used in the calculation of the blackbody shift. Presently, we report a fractional blackbody shift correction of  $-21.21 \times 10^{-15}$  calculated using the accepted coefficients and expression [1] with an uncertainty in the correction of  $0.26 \times 10^{-15}$  corresponding to  $\pm 1$  K.

#### 4.4. Gravitational redshift

Although the gravitational redshift is the largest correction applied to NIST-F1, the reported fractional uncertainty has been negligible at  $\pm 1.0 \times 10^{-16}$  [12]. A more recent model of the geoid [13] will allow the correction to be applied in future accuracy evaluations of NIST-F1 with an uncertainty of  $\pm 0.3 \times 10^{-16}$ .

## 5. Uncorrected frequency biases

### 5.1. Second-order Doppler shift

The fractional frequency shift due to the second-order Doppler effect under standard operating conditions in NIST-F1 is calculated to be  $-1.4 \times 10^{-17}$ . While this shift is presently not included in the corrected biases, if required, it is possible to correct for a very small uncertainty since the launch velocity of the atoms, the local value of  $g$  and the total ballistic flight time of the atoms are well known.

### 5.2. Rabi pulling

Rabi pulling is a line-shape effect due to the tails of adjacent  $\sigma(\Delta m = 0)$  microwave transitions overlapping with the central  $|3, 0\rangle \rightarrow |4, 0\rangle$  clock transition. In fountains such as NIST-F1, using microwave state-selection and an optical pulse to remove the residual  $m_F \neq 0$  levels, this shift is very small. Experimental data discussed in [1] show the fractional frequency shift due to Rabi pulling in NIST-F1 to be of the order of  $10^{-19}$ .

### 5.3. Ramsey pulling

Ramsey pulling is a lineshape bias due to undesired  $\Delta m = \pm 1$  transitions to or from one of the  $m = 0$  clock transition sublevels and is expected to be small in fountains where the state-selection is  $m_F$  sensitive [1]. A recent re-analysis of Ramsey pulling in NIST-F1 using the theory outlined in [14] shows the fractional frequency shift to be of the order of  $\approx 10^{-19}$ .

### 5.4. Majorana transitions

Majorana transitions cause frequency shifts in magnetically state-selected beam frequency standards due to the different trajectories of the various  $m_F$  levels in Cs [15]. However, the optical detection scheme used in NIST-F1 is insensitive to the  $m_F$  state of an atom. Therefore, Majorana transitions result in only a loss of contrast in the Ramsey fringes. Since the loss of contrast will be symmetric about the central fringe, an overall frequency bias is not expected. As discussed in [1], even assuming an unphysical 100% asymmetry in the probability of Majorana transitions about the central Ramsey fringe, the expected fractional frequency shift in NIST-F1 is no larger than  $2 \times 10^{-17}$ .

### 5.5. Microwave power-dependent shifts including distributed cavity phase and microwave leakage

Microwave power-dependent shifts in NIST-F1 are evaluated by performing Ramsey spectroscopy at odd multiples of the nominal  $\pi/2$ -pulse excitation level, typically up to a  $9\pi/2$ -pulse. We have never reported a systematic bias due to microwave power, and the associated Type B uncertainties have been limited by the length of data collection periods.

A recent analysis [16] shows that the distributed cavity phase is a function of microwave power levels within the cavity. In light of this treatment, we are reconsidering the methods by

which the bias is evaluated. This analysis shows that since the field in the cavity is the sum of a real standing-wave component and a much smaller imaginary travelling component due to losses (resulting in a distributed cavity phase shift), as the power level is increased through multiple  $\pi/2$  excitations, the out-of-phase imaginary component adds to the total field, with the result that the frequency bias oscillates in sign and magnitude with increasing power. Until tests of this new analysis are complete, an uncertainty of  $2 \times 10^{-17}$  is assigned to the bias due to distributed cavity phase which is based on the worst-case arguments presented in [1].

Similar techniques have been applied to the problem of microwave leakage [17], a serious concern in atomic standards and lacking complete theoretical treatment. This work shows that for microwave leakage to result in a frequency bias, the leakage field must have a complex phase with respect to the microwave field in the Ramsey cavity. Additionally, the leakage field amplitude must have an antisymmetric component with respect to the Ramsey interrogation time. Given these conditions, the bias due to leakage can be measured by varying the microwave power in the Ramsey cavity through multiple  $\pi/2$  excitations. As with the case described above with distributed cavity phase, the out-of-phase field component due to leakage adds to the field in the Ramsey cavity such that the bias oscillates with increasing power. Table 1 shows no frequency bias due to microwave leakage within the fractional uncertainty of  $0.2 \times 10^{-15}$ . This uncertainty is limited by the amount of time spent collecting frequency measurements at various microwave power levels and was obtained using the new analysis [17] discussed above.

### 5.6. Cavity pulling

First-order cavity pulling is due to the interaction of the oscillating magnetization of the atomic sample with the microwave field within the cavity resulting in a phase shift in the excitation field and therefore a frequency shift in the atomic transition. This effect has been studied thoroughly in masers [18] and more recently in Rb fountains [19, 20], where it is a large effect due to the high atomic densities and large cavity detunings. In NIST-F1 the first-order cavity pulling is small because the densities are a factor of  $\sim 10^3$  lower than described in [19]. Also, the microwave cavity is temperature stabilized such that the cavity resonance is much less than one linewidth away from the atomic transition. An analysis using the techniques outlined in [18, 19] places the fractional shift due to first-order cavity pulling at the  $10^{-18}$  level.

Second-order cavity pulling is a sloping baseline bias due to operating the Ramsey microwave cavity off the atomic resonance in unison with the microwave power not being optimized for  $\pi/2$  transitions on resonance [15]. In this situation, microwave power as seen by the atoms is coupled to the resonance response curve of the Ramsey cavity. The effect vanishes when either the power is optimized or the cavity is exactly on resonance, neither of which is possible in practice. In NIST-F1 the microwave power is set to within  $\pm 0.1$  dB of optimum by measuring the amplitude of the  $F = 3$  peak as a function of power until the minimum is located. The power levels are checked using this procedure

approximately every 24 h and are stable at this level. Also, the cavity detuning from the atomic resonance is less than one cavity linewidth. Using these values and the arguments presented in [15] (equation 5.6.123) the bias is estimated to be less than  $2 \times 10^{-17}$ . This effect is uncorrected for in the uncertainty budget.

### 5.7. Fluorescence light shifts

The improved optical and mechanical shutter system described in section 2.2 has allowed for a more controlled method to measure the fluorescent light shift. NIST-F1 was operated with the mechanical shutters fixed in the open position and a resulting fractional shift of  $\sim 8 \times 10^{-14}$  was measured. This bias was then divided by the attenuation factor of the new shutters, which was measured to be  $> 10^7$ . This result shows the fractional fluorescent light shift to be  $\sim 10^{-20}$ .

### 5.8. Integrator offset

The new software that operates the NIST-F1 line-centre servo was tested for offsets by alternating between the old software and the new software over 18 days. The measured fractional frequency offset between operation with the new and the old software routines is  $-0.35(76) \times 10^{-15}$ . This shows no difference between the results from the two programs within the uncertainty of the measurement, which is limited by the run length. A second test of the new software involved operating NIST-F1 normally, except with no atom signal, and found no integrator offset within the  $1 \times 10^{-17}$  uncertainty of the measurement. We view these measurements as a precautionary exercise since we have no logical reason to expect a bias between the two software routines since the core line-centre servo algorithms are very simple and mathematically identical. Nevertheless, the above uncertainty, limited by measurement times, will be further reduced by continued measurements.

### 5.9. Microwave spectrum

The microwave synthesizers described in section 2.5 have similar architectures in that the phase noise close to the carrier is dominated by the DDS module, which is mixed in by use of an SSB mixer on the output stage. This DDS has been evaluated at NIST [21] and measurements presented in [1] place the frequency bias due to spectral impurities at less than  $3 \times 10^{-18}$ .

### 5.10. The dc Stark shift

The Ramsey microwave cavity and time of flight tube are constructed of oxygen-free high-purity copper components that have been brazed together and are therefore at the same nominal dc potential. However, small thermoelectric currents across the braze joints create potential differences, but they are exceedingly small. Stray potentials from insulating 'spots' such as frozen solvents, etc on the vacuum walls are not expected in NIST-F1 due to careful UHV techniques used on the vacuum system. Also, there is no source of charged particles within the physics package to keep such an insulating spot continuously charged. Finally, patch potentials due to macroscopic variations in the crystalline structure in the

copper walls of the Ramsey and time of flight tube can exhibit surprisingly large potentials of  $\sim 0.01$  V, but only on a length scale of  $10^{-6}$  m along the surface [22]. These potentials can make large fields, but only on a very small spatial scale and therefore do not extend into the trajectory of the Cs atoms. Throwing aside these arguments for a negligible shift, we can estimate the size of a dc Stark shift assuming an unphysical, worst-case scenario. Assume a patch charged to 1 V in the toss tube located at the apogee of the atomic trajectory. Such a patch would generate a field of the order of  $100 \text{ V m}^{-1}$ , and the interaction with the atomic sample would be approximately 100 ms. Using the coefficients published in [23], the fractional shift is calculated to be  $\sim 2 \times 10^{-17}$ .

### 5.11. Collisions with background gases

The hyperfine pressure shift in Cs has been measured for a variety of gases in buffer cells [24, 25]. New vacuum pressure instrumentation recently installed on NIST-F1 is sensitive down to  $5 \times 10^{-15}$  Torr ( $6.6 \times 10^{-13}$  Pa). Although this gauge is in a location that has low conductance to the Ramsey interrogation region, it nevertheless gives us an estimate of the vacuum environment within the physics package. This gauge indicates a base pressure of  $5 \times 10^{-12}$  Torr ( $6.6 \times 10^{-10}$  Pa), even while the Cs oven is on. This indicates that the large amount of graphite getters between the source and the rest of the vacuum system efficiently removes the Cs. Assuming there is a background in the Ramsey region of exclusively  $\text{H}_2$ , which has a large pressure shift of  $1.08 \times 10^3 \text{ Hz Torr}^{-1}$  ( $8.12 \text{ Hz Pa}^{-1}$ ), this puts the fractional shift at  $\approx 1 \times 10^{-18}$ . Given the symmetry of the vacuum system, we are confident that the measurements at the ion gauge give a reasonable estimate of the pressure within the microwave cavity structure and the time of flight tube above the cavity.

### 5.12. Bloch–Siegert shift

The linearly polarized microwave field that drives the hyperfine clock transition must be viewed as the resultant of two counter-rotating fields with circular polarization. Although only one of these fields is significant (the rotating-wave approximation), the frequency bias due to the second component (the Bloch–Siegert shift) must be considered in NIST-F1. The fractional frequency bias at normal Ramsey microwave power levels ( $\pi/2$ ) was determined [15] (equation 5.6.93) to be negligible at  $\approx 10^{-19}$ . At a microwave power level of  $5\pi/2$ , the shift remains small at  $\approx 3 \times 10^{-18}$ . The Bloch–Siegert shift remains negligible even with the improved accuracy afforded in laser-cooled Cs fountains since it scales inversely with the atomic line  $Q$  and decreases with microwave field strength.

## 6. Evaluation procedure

A typical evaluation of NIST-F1 begins with tuning up the entire system for maximum performance over the span of approximately one week. Checks are performed on critical systems such as the physics package temperature controller, microwave monitor, mechanical light shutters, etc. Next, the magnetic field is mapped using the techniques described

in section 4 and in [1] to correct for the second-order Zeeman shift. Other leveraged measurements of systematic biases, such as microwave power shifts, are performed. Next, frequency data are collected at the low atomic density set point for  $\sim 10$  days. A transition is then made to medium atomic density by making small changes to several systems: the Cs oven temperature, optical molasses laser power and molasses load time. The parameters are adjusted such that the atom-number servo operates at approximately the same microwave power incident on the state-selection cavity. NIST-F1 is operated at medium atomic density for several days. This procedure is repeated for the transition to high atomic density and data are collected for several days. Finally, we return to medium density for a few days and then back to low atomic density for another  $\sim 10$  days of operation. In practice, the exact length of an evaluation will vary depending on many factors. Also, operating NIST-F1 at the various densities in the time sequence described above, symmetrically about the midpoint of the evaluation interval, minimizes the impact of any linear frequency drift in AT1E.

The data collected during an evaluation are a record of the frequency of a reference maser in the NIST clock ensemble against the Cs clock transition with systematic biases, including a time-varying Cs collisional shift. The raw data are processed to reference it against AT1E, which is more stable than the single reference maser. A weighted, least-squares linear fit of the data (atomic density versus frequency) yields an intercept which is the Cs clock transition with no collisional shift. This process is described in more detail in [2]. Other corrections for systematic biases are applied to this resulting frequency. The final uncertainty budget is shown in table 1. The submission of the final result to the BIPM requires a discussion of the time-transfer system which is presented in the next section.

## 7. Time transfer

The stability of AT1E also allows for results of an evaluation of NIST-F1 to be effectively extended or ‘stretched’ in time to reduce the uncertainty of the time-transfer process used to submit NIST-F1 measurements into TAI. The noise characteristics of the time-transfer process are such that the frequency uncertainty in the transfer process is given as  $u_{\text{Link}/\text{TAI}} = 3 \times 10^{-14}/\tau$  for  $\tau$  in days. Thus a report interval of 30 days is required to reduce the fractional uncertainty in the transfer process to  $\sim 1 \times 10^{-15}$  [2]. Since the accuracy of the fountain can be determined at the  $\sim 10^{-15}$  level in approximately 10 days, the timescale is used to hold on to these accuracies until the uncertainty in the time-transfer process decreases to an acceptable level. In practice, an evaluation of NIST-F1 is ‘stretched’ by adding dead time onto both the beginning and end until the uncertainty in the time-transfer process during the final reporting interval is about the same as the uncertainty due to the total dead time. As a result, the NIST-F1 frequency data are submitted into TAI with a smaller uncertainty than without ‘stretching’ the run interval.

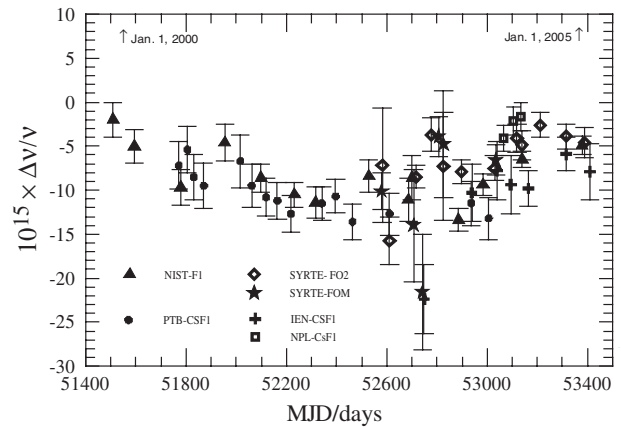


**Figure 5.** A plot showing over four years of TAI versus data from fountain primary frequency standards taken from *Circular T* and the *Annual Report of the Time Section* of the BIPM. In addition to NIST-F1, contributions are shown from PTB-CSF1, two standards from SYRTE, SYRTE-FO2 and SYRTE-FOM (a transportable fountain), IEN-CSF1 and NPL-CsF1, all caesium fountains. The horizontal axis is given in days in terms of the MJD. There are several years of fairly regular data from NIST-F1 and PTB-CSF1 that show very good agreement. Several of the contributions from SYRTE and IEN are difficult to compare with the rest of the data given the rather large reported uncertainties.

## 8. NIST-F1 performance assessment and comparison with other Cs fountains

Since the publication of [1] much more data from Cs fountain primary standards have become available for comparisons. Figure 5 shows over four years of data from primary standards taken from *Circular T* and the *Annual Report of the Time Section* of the BIPM. In addition to NIST-F1, contributions are shown from the fountain at Physikalisch-Technische Bundesanstalt (PTB), PTB CSF1, two fountains at Systèmes de Référence Temps Espace (SYRTE), SYRTE-FO2 and SYRTE-FOM, the fountain at Istituto Elettrotecnico Nazionale (IEN), IEN-CSF1, and most recently, the fountain at National Physical Laboratory (NPL), NPL-CsF1. The horizontal axis is given in days in terms of the Modified Julian Date (MJD). There are several years of fairly regular data from NIST-F1 and PTB-CSF1 that show very good agreement. Several of the contributions from SYRTE and IEN are difficult to compare with the rest of the data, given the relatively large reported uncertainties. However, the data submitted within the last year from NIST-F1, SYRTE and IEN all show good agreement.

## 9. Conclusion

Table 3 shows a complete breakdown of the uncertainties from three formal accuracy evaluations of NIST-F1 and highlights the improvements discussed in this paper. The first evaluation is from July 2001 and the other two, more recent, evaluations are from June 2004 and January 2005. The Type A uncertainties shown in table 3 have been broken down into the components due to statistics and the components due to the spin-exchange bias [2] to clearly illustrate that both have reduced in magnitude. Although the dead-time uncertainties,  $u_{\text{Link}/\text{Lab}}$ , are larger for the most recent evaluations due to

intentionally added dead time, there is a net benefit because the uncertainty due to the time transfer,  $u_{\text{Link}/\text{TAI}}$ , decreases.

Presently, the leading item in the Type B uncertainty budget is the blackbody radiation shift. It is unlikely that a significant reduction in this uncertainty is possible with NIST-F1. Rather, this shift will be addressed with NIST-F2, under development at NIST, which has a cryogenic Ramsey interrogation region. Even as NIST-F2 develops into a primary standard, NIST-F1 will remain operational at NIST, both as a tool for the evaluations of NIST-F2 and as an additional standard for the NIST timescale and the BIPM.

## References

- [1] Jefferts S R *et al* 2002 *Metrologia* **39** 321–36
- [2] Parker T E, Jefferts S R, Heavner T P and Donley E A 2005 *Metrologia* **42** 423–30
- [3] Parker T E 1999 *Proc. 1999 Joint Meeting IEEE Int. Freq. Control Symp. and EFTF Conf. (Besançon)* pp 173–6
- [4] Howe D A and Pepler T K 2003 *Proc. 2003 Joint Meeting IEEE Int. Freq. Control Symp. and EFTF Conf. (Tampa, FL)* pp 233–8
- [5] Nava J H, Walls F L, Shirley J H, Lee W D and Armburo M M 1996 *Proc. 1996 IEEE Int. Freq. Control Symp. (Honolulu, HI)* pp 973–9
- [6] Jefferts S R, Heavner T P, Donley E A and Parker T E 2004 *IEEE Trans. Ultrason. Ferroelec. Freq. Control* **51** 652–3
- [7] Parker T E 2001 *Proc. 2001 IEEE Int. Freq. Control Symp. (Seattle, WA)* pp 57–62
- [8] Leo P J, Julienne P S, Mies F H and Williams C J 2001 *Phys. Rev. Lett.* **86** 3743–6
- [9] Pereira Dos Santos F, Marion H, Bize S, Sortais Y and Clairon A 2002 *Phys. Rev. Lett.* **89** 233004
- [10] Taylor B N and Kuyatt C E 1993 *Guidelines for Evaluating and Expressing the Uncertainty of NIST Measurement Results, NIST Technical Note 1297*
- [11] Micalizio S, Godone A, Calonico D, Levi F and Lorini L 2004 *Phys. Rev. A* **69** 053401
- [12] Weiss M A and Ashby N 2000 *Metrologia* **37** 715–17
- [13] Pavlis N K and Weiss M A 2003 *Metrologia* **40** 66–73
- [14] Shirley J H, Lee W D and Drullinger R E 2001 *Metrologia* **38** 427–58
- [15] Vanier J and Audoin C 1989 *The Quantum Physics of Atomic Frequency Standards* (Bristol: Hilger) p 836
- [16] Jefferts S R, Shirley J H, Burt E and Dick G J 2005 *IEEE Trans. Ultrason. Ferr.* at press
- [17] Jefferts S R, Shirley J H, Ashby N, Heavner T P, Donley E A, Levi F, Burt E A and Dick G J 2005 *Proc. 19th Eur. Time and Frequency Forum (Besançon)* at press
- [18] Wineland D J and Ramsey N F 1972 *Phys. Rev. A* **5** 821–37
- [19] Bize S, Sortais Y, Mandache C, Clairon A and Salomon C 2001 *IEEE Trans. Instrum. Meas.* **50** 503–6
- [20] Fertig C and Gibble K 2000 *Phys. Rev. Lett.* **85** 1622–5
- [21] Lee W D, Shirley J H, Walls F L and Drullinger R E 1995 *Proc. 1995 IEEE Int. Freq. Control Symp. (San Francisco, CA)* pp 113–18
- [22] Rossi F and Opat G 1992 *J. Phys. D: Appl. Phys.* **25** 1349–53
- [23] Simon E, Laurent P and Clairon A 1998 *Phys. Rev. A* **57** 436–9
- [24] Beer C W and Bernheim R A 1976 *Phys. Rev. A* **13** 1052–7
- [25] Arditì M and Carver T R 1961 *Phys. Rev.* **124** 800–9